to CR9114 (table S7) (*7*). The other Ile45Phe escape variant is naturally present in essentially all human H2N2 viruses that circulated from 1957 to 1968, and Phe45Ile substitution in a human H2 HA restores high affinity binding for both CR6261 and CR9114 (table S8). In contrast, Phe^{45} occurs in only 3 of 8550 sequences from avian H2N2 isolates and the remaining 15 subtypes.
31. J. C. Krause *et al*., *J. Virol.* **85**, 10905 (2011).
32. J. R. Whittle *et al*., *Proc. Natl. Acad. Sci. U.S.A.* **108**, 14216 (2011).
33. Why influenza B viruses are not neutralized in the same way by CR9114 remains currently unknown.
34. In contrast, polyclonal sheep sera directed against B/Florida/4/2006 and B/Malaysia/2506/2004 did prevent initial infection, but not of virus from the opposite lineage.
35. L. V. Gubareva, L. Kaiser, F. G. Hayden, *Lancet* **355**, 827 (2000).
36. Y. Bao *et al*., *J. Virol.* **82**, 596 (2008).

Acknowledgments: We thank J. Juraszek; B. Brandenburg; M. Koldijk; K. Hegmans; J. Meijer; N. Hafkemeier; A. Apetri; J. Dulos; L. Dekking; H. Vietsch; G. Perdok; H. Tien; D. Marciano; the staff of the Advanced Photon Source (APS) GM/CA-CAT 23ID-B and 23ID-D, Stanford Synchrotron Radiation Lightsource (SSRL) BL11-1 and SSRL BL7-1, and Advanced Light Source (ALS); X. Dai; R. Stanfield; W. Yu; J. P. Julien; R. N. Kirchdoerfer; and E. Brown of Ottawa University, Canada, for the mouse-adapted A/Hong Kong/1/68 strain. Crystallization experiments were carried out on the Rigaku Crystalmation system at the Joint Center for Structural Genomics, which is supported by the National Institute of General Medical Sciences (NIGMS) Protein Structure Initiative U54 GM094586. The EM and image analysis was conducted by R.K., J.H.L., and Z.M. at the National Resource for Automated Molecular Microscopy, which is supported by NIH through the National Center for Research Resources' P41 program (RR017573). This project has been funded in part by the Area of Excellence Scheme of the University Grants Committee, Hong Kong (grant AoE/M-12/06); a predoctoral fellowship from the Achievement Rewards for College Scientists Foundation (D.C.E.); grant GM080209 from the NIH Molecular Evolution Training Program (D.C.E.); a Saper Aude Postdoc grant from the Danish Council for Independent Research, Natural Sciences (N.S.L.), and the Skaggs Institute (I.A.W.). Portions of this research were carried out at the SSRL, a national user facility operated by Stanford University on behalf of the U.S. Department of Energy (DOE), Office of Basic Energy Sciences. The SSRL Structural Molecular Biology Program is supported by the DOE Office of Biological and Environmental Research and by NIH, National Center for Research Resources, Biomedical Technology Program (P41RR001209), and the NIGMS. The GM/CA CAT 23-ID-B beamline has been funded in whole or in part with federal funds from National Cancer Institute (Y1-CO-1020) and NIGMS (Y1-GM-1104). Use of the APS was supported by the DOE, Basic Energy Sciences, Office of Science, under contract no. DE-AC02-06CH11357. The content is solely the responsibility of the authors and does not necessarily represent the official views of NIGMS or the NIH. The ALS is supported by the director, Office of Science, Office of Basic Energy Sciences, of the DOE under contract no. DE-AC02-05CH11231. Coordinates and structure factors are deposited in the Protein Data Bank (PDB code 4FQH for CR9114 Fab, 4FQI for CR9114 Fab-A/H5 HA, 4FQJ for CR8071 Fab-B/Florida HA1, 4FQK for CR8059 Fab-B/Brisbane HA, 4FQL for CR8033 Fab, 4FQM for B/Brisbane HA, 4FQY for CR9114 Fab-A/H3 HA, and 4FQV for CR9114 Fab-A/H7 HA). Image reconstructions have been deposited at the EMDataBank under accession numbers EMD-2143 (CR8033/Florida), EMD-2144 (CR8071/Florida), EMD-2145 (CR8071/Malaysia), EMD-2146 (CR9114/Florida), EMD-2147 (CR9114/H1), EMD-2148 (CR9114/H3), EMD-2149 (CR9114/H9), and EMD-2150 (CR9114/H7). Nucleotide sequences for the CR8033, CR8059 (CR8071), and CR9114 variable regions have been deposited in GenBank [accession numbers JX213635 (CR8033, V_H), JX213636 (CR8033, V_κ), JX213637 (CR8059, V_H), JX213638 (CR8059, V_λ), JX213639 (CR9114, V_H), and JX213640 (CR9114, V_λ)]. Patent applications relating to antibodies CR8033, CR8059, CR8071, and CR9114 have been filed (CR8033, CR8059, and CR8071 are claimed in EP 12158525.1 and U.S. 61/608,414. CR9114 is claimed in EP 11173953.8 and U.S. 61/572,417). Sharing will be subject to standard material transfer agreements. This is publication 21741 from the Scripps Research Institute.

Supplementary Materials
www.sciencemag.org/cgi/content/full/science.1222908/DC1
Materials and Methods
Figs. S1 to S18
Tables S1 to S8
References (*37*–*62*)

4 April 2012; accepted 9 July 2012
Published online 9 August 2012;
10.1126/science.1222908

Structural Probing of a Protein Phosphatase 2A Network by Chemical Cross-Linking and Mass Spectrometry

Franz Herzog,[1]* Abdullah Kahraman,[1]* Daniel Boehringer,[2]* Raymond Mak,[1] Andreas Bracher,[4] Thomas Walzthoeni,[1] Alexander Leitner,[1] Martin Beck,[3] Franz-Ulrich Hartl,[4] Nenad Ban,[2] Lars Malmström,[1] Ruedi Aebersold[1]†

The identification of proximate amino acids by chemical cross-linking and mass spectrometry (XL-MS) facilitates the structural analysis of homogeneous protein complexes. We gained distance restraints on a modular interaction network of protein complexes affinity-purified from human cells by applying an adapted XL-MS protocol. Systematic analysis of human protein phosphatase 2A (PP2A) complexes identified 176 interprotein and 570 intraprotein cross-links that link specific trimeric PP2A complexes to a multitude of adaptor proteins that control their cellular functions. Spatial restraints guided molecular modeling of the binding interface between immunoglobulin binding protein 1 (IGBP1) and PP2A and revealed the topology of TCP1 ring complex (TRiC) chaperonin interacting with the PP2A regulatory subunit 2ABG. This study establishes XL-MS as an integral part of hybrid structural biology approaches for the analysis of endogenous protein complexes.

Cellular processes can rarely be attributed to the activity of a single protein. Instead, proteins act in functional modules, such as macromolecular complexes or signal transduction networks. Gaining mechanistic insights into the function of multisubunit modules is facilitated by structural elucidation (*1*, *2*). Chemical cross-linking, in combination with mass spectrometry (XL-MS), is a low-resolution structural technique for the characterization of the architecture of protein complexes (*3*, *4*). XL-MS provides distance information by identifying spatially proximate lysine residues that have been covalently linked by a bifunctional cross-linking reagent. This approach has been successfully applied to homogenous protein complexes purified for crystallographic purposes (*5*–*8*). In contrast to high-resolution structural biology techniques, XL-MS has the potential to acquire spatial restraints from heterogeneous protein samples. We thus applied this method to characterize the topology of a signaling network by systematic analysis of endogenous protein complexes (Fig. 1).

The abundant protein phosphatase 2A (PP2A) is involved in diverse signaling pathways regulating cell growth, apoptosis, differentiation, cell motility, DNA damage response, and cell cycle progression (*9*–*12*). In eukaryotes, active PP2A holoenzymes are heterotrimers composed of a catalytic subunit (C, human isoforms PP2AA and PP2AB), a scaffold subunit (A, human isoforms 2AAA and 2AAB), and one of a large array of regulatory subunits (B, B', B", and B"', each subfamily consisting of two to five isoforms) (Fig. 2A and table S1) that selectively target PP2A subpopulations to specific substrates (*13*). To reveal the topology of PP2A holoenzymes in complex with the adaptor proteins that regulate their phosphatase activity and subcellular location, we purified these complexes from human cells and analyzed their topology by combining XL-MS and computational molecular modeling.

We first determined the proteins copurifying with trimeric PP2A holoenzymes by isolating 14 proteins, previously detected in PP2A complexes (*14*, *15*), through an N-terminal His_6-HA-StrepII-tag from human embryonic kidney cells (fig. S1 and table S2). The associated protein complexes were identified by mass spectrometry (Fig. 1) (*16*), resulting in a dense interaction network of 94 proteins (Fig. 2A and tables S1 and S3).

To elucidate the topology of the PP2A network, we probed the complexes by XL-MS. Cross-linking was achieved by immobilizing the PP2A complexes on beads (*16*). Incubation with the appropriate concentration of disuccinimidyl suberate (DSS) (fig. S2) and subsequent proteolysis resulted in a complex mixture of tryptic peptides that was

[1]Department of Biology, Institute of Molecular Systems Biology, Eidgenössische Technische Hochschule Zürich, Wolfgang-Pauli Strasse 16, 8093 Zurich, Switzerland. [2]Department of Biology, Institute of Molecular Biology and Biophysics, Eidgenössische Technische Hochschule Zürich, Schafmattstrasse 20, 8093 Zurich, Switzerland. [3]European Molecular Biology Laboratory, Meyerhofstraße 1, 69117 Heidelberg, Germany. [4]Department of Cellular Biochemistry, Max Planck Institute of Biochemistry, Am Klopferspitz 18, 82152 Martinsried, Germany.

*These authors contributed equally to this work.
†To whom correspondence should be addressed. E-mail: aebersold@imsb.biol.ethz.ch

analyzed by tandem mass spectrometry (*17*). Cross-linked peptides were identified by the search engine xQuest (*3*, *16*, *18*) (Fig. 1 and fig. S3).

XL-MS analyses of the PP2A complexes associated with the 14 bait proteins were performed at least in duplicate (table S2) and yielded 176 interprotein (Fig. 2B) and 570 intraprotein cross-links. As various interactions were repeatedly detected within the PP2A network, we further assessed the confidence of cross-link identifications by counting the number of fragment ion spectra in the data set and the number of experiments detecting a specific cross-link (tables S4 and S5).

Cross-link assignments were further evaluated by measuring the distances between the two lysine residues on x-ray structures and comparative models of the human protein complexes identified in the PP2A network (fig. S4 and tables S4 to S6) (*16*). The median Euclidean Cα-Cα distances for the charted 70 interprotein and 287 intraprotein peptide pairs were 19.6 Å and 15.4 Å, respectively (Fig. 2C). Of these cross-links, 92% were below 30 Å, the estimated maximum threshold for the Euclidean distance spanned by DSS, accounting for protein dynamics and model inaccuracies (fig. S5) (*16*). Thus, cross-link–derived spatial restraints can guide computational modeling and protein-protein docking studies.

The closest human relatives of the PP2A catalytic subunits within the phosphoprotein phosphatase family are PP4C and PPP6 (*11*). Reciprocal pull-downs of 2A5D, PP2AA, and PP4C indicate that subunits of PP2A and PP4 copurify (Fig. 2A and table S3) (*19*). Cross-links suggest that P4R3A, the regulatory subunit of PP4, occupies a position similar to the regulatory B' subunit 2A5G on the PP2A scaffold subunit 2AAA, thus assembling a P4R3A/2AAA/PP4C hybrid complex (Fig. 2B and tables S3 and S4) (*20*).

The catalytic subunits PP2AA, PP2AB, PP4C, and PPP6 were previously shown to form heterodimeric complexes with immunoglobulin binding protein 1 (IGBP1), which inactivates the catalytic subunits and prevents their proteasomal degradation until functional phosphatase complexes are assembled (*21*). Previous binding studies revealed that residue E42 of PP2AA (*22*) and residues R155 and K158 of IGBP1 (*23*, *24*) are essential for the interaction of IGBP1 with the catalytic subunits. To locate the binding interface between IGBP1 and the catalytic subunits PP2AA and PP4C, we used seven and three interprotein restraints, respectively, to guide molecular modeling. Starting from the crystal structure of the N-terminal 221 amino acids of mouse IGBP1 (*23*), we first localized the C-terminal domain within a full-length human structural model of IGBP1 by de novo modeling using the Rosetta software suite (*25*) and intraprotein cross-links, including 18 within the C terminus and 32 between the C- and N-terminal domains (fig. S6 and table S7) (*16*). Protein structures of PP2AA and IGBP1 were subjected to the docking protocol of Rosetta (*26*), resulting in 1075 docking models that clustered into 237 groups (Fig. 3A). The 300 docking models with the shortest average distance for the seven identified IGBP1-PP2AA cross-links clustered into four large groups (Fig. 3B) (*16*). This strategy yielded a defined 1447 $Å^2$ binding interface displaying residues E37 of PP2AA and K163 of IGBP1 at the interface in 95% of the docking models (Fig. 3C; fig. S7, A and B; figs. S8 to S10; and table S8). The interface to PP4C was less constrained because it was defined by only three distance restraints (fig. S7, C to F, and tables S9 and S10) (*16*). We detected the previously identified interface residues E42 of PP2AA (*22*) at a frequency of 32% and R155 and K158 of IGBP1 (*23*, *24*) in 43% and 5% of the modeled interfaces, respectively (Fig. 3C and table S11). Mutating K163 in IGBP1 to alanine reduced binding to the PP2A catalytic subunits compared with wild-type IGBP1 (Fig. 3D). The R155A IGBP1 mutant completely abrogated interaction, whereas the K158A mutant still bound residual amounts of the catalytic subunits that were further reduced by K158A/K163A double mutation. These results indicate that K163 of IGBP1, the interface residue most frequently mapped in computational docking experiments, is involved in forming the binding interface with the catalytic PP2A subunits. Consistent with previous studies, we found that binding of IGBP1 and of the PP2A scaffold subunits to the catalytic subunits is mutually exclusive (Fig. 2A and table S3) and that their binding sites on PP2AA minimally overlap (fig. S11) (*22*). IGBP1 binding may thus prevent interaction of PP2A catalytic and scaffold subunits by steric hindrance and allosteric distortion of the catalytic-scaffold interface rather than by direct competition with the scaffold subunit (*21*).

Interprotein cross-links unveiled the topology of PP2A complexes mediated by distinct regulatory subunits, such as the B"'/striatin-interacting phosphatase and kinase (STRIPAK) complex (Fig. 3E) (*14*). P2R3C (B") linked PP2A activity to the centrosomal complex CE350/FR1OP (*27*) and B and B' subunits were found to be cross-linked to the Integrator complex (*14*) (Fig. 2B). Covalent linkages indicated that B' proteins recruit PP2A to several adaptor proteins such as LIP1, PRR14, FA13A, and CCDC6 and to a distinct set of cell cycle regulators, including M89BB, ESPL1, and SGOL1 (Fig. 2B and table S4).

SGOL1 specifically targets A/B'/C complexes to centromeres, which are thought to dephosphorylate cohesin and thereby prevent precocious cohesin dissociation in mitosis and meiosis (*28*, *29*). Previous x-ray structure determination of a PP2A-SGOL1 complex revealed that residues 51 to 96 of SGOL1 form a parallel homodimeric coiled coil, which is a prerequisite for its binding to PP2A holoenzymes. The N- and C-terminal ends of SGOL1 helices form discrete interfaces with PP2AA and 2A5G, respectively (*30*). On SGOL1-bound PP2A complexes, we identified 11 SGOL1 intraprotein cross-links and two and three interprotein cross-links to PP2A C or B' subunits, respectively (Fig. 2B and tables S4 and S5). SGOL1 also copurified with the PP2A inhibitor SET and

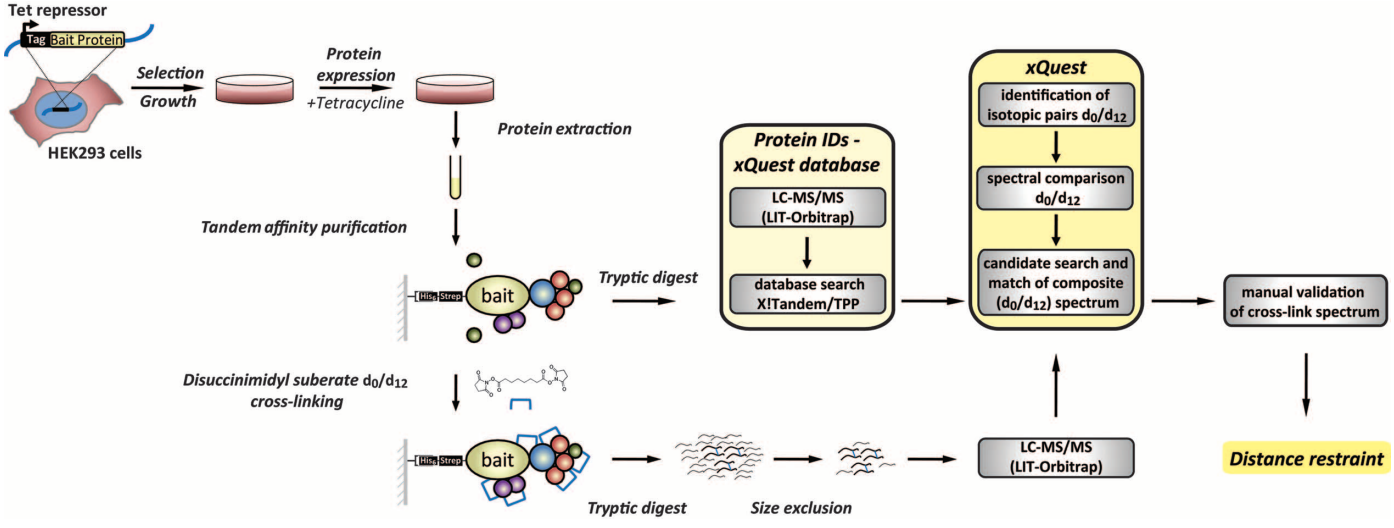

Fig. 1. Schematic outline of the XL-MS workflow established for the identification of chemically cross-linked lysines on affinity-purified human PP2A complexes (*16*). LC-MS/MS, liquid chromatography coupled to tandem mass spectrometry; LIT, linear ion trap; TPP, trans-proteomic pipeline.

the SGOL1-SET complex was characterized by seven interprotein cross-links (Fig. 3F). Interestingly, the x-ray structure of the SET-TAF1β complex revealed an extended N-terminal helix (33 to 90) undergoing coiled-coil interactions in SET (*31*), which is of similar length as the SGOL1 helix. It is thus conceivable that a similar coiled-coil interface might be established in the SGOL1-SET complex. The distribution of cross-links between SGOL1 and SET residues suggests an antiparallel arrangement (Fig. 3F) that reveals an array of hydrophobic residues similar to the hydrophobic interactions mediating SGOL1 homodimer formation (Fig. 3, G and H) (*30*). Together with the observation that SET and SGOL1 copurify with the B' subunit 2A5E (Fig. 2A and table S3) (*28*), our cross-links suggest that SGOL1 may be involved in recruiting the PP2A inhibitor SET to the catalytic center of PP2A holoenzymes or in maintaining SET binding.

The WD40 propeller-containing regulatory subunits, B and B"', which are presumably in a partially folded state, were found to be cross-linked to subunits of TCP1 ring complex (TRiC), a cylindrical molecular chaperone complex consisting of two hetero-octameric rings (Fig. 2B and table S4) (*32*). We identified 54 TRiC intersubunit cross-links consistent with the recently reported subunit topology (Fig. 4A and fig. S4C) (*33*, *34*) and demonstrating that we purified the fully assembled chaperone complex. Isolating TRiC in a stoichiometric complex with endogenous 2ABG (fig. S12) facilitated the identification of 19 cross-links between 2ABG and the N- and C-terminal tails of TRiC subunits, which are located in the equatorial domains (Fig. 4, B and C). Minimizing the distance restraints placed 2ABG at the equatorial plane in the inner cavity of the octameric TRiC ring (Fig. 4C and fig. S13)

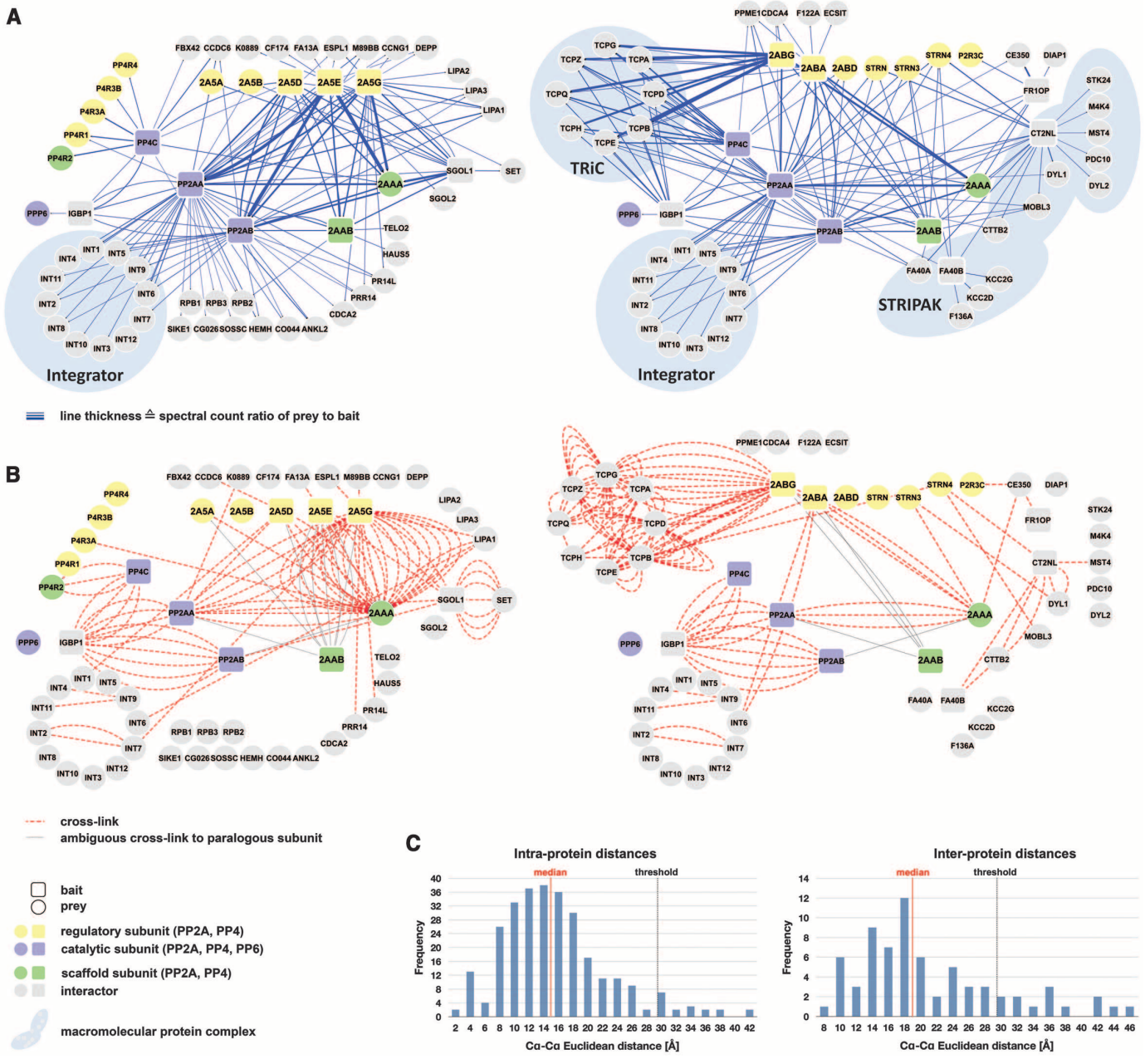

Fig. 2. Identification of interprotein distance restraints on PP2A protein complexes by XL-MS. (**A**) PP2A protein interaction network based on reciprocal pull-down assays. (**B**) PP2A network topology represented by interprotein cross-links. [(A) and (B)] Network is split according to PP2A regulatory subunits. B' (2A5A, 2A5B, 2A5D, 2A5E, and 2A5G) subunits are shown in the left panel and B (2ABA, 2ABD, and 2ABG), B" (P2R3C) and B"' (STRN, STRN3, and STRN4) in the right panel. (**C**) Histogram of the Euclidean Cα-Cα distances between cross-linked lysines determined on x-ray structures and comparative models of the PP2A network. Threshold, estimated maximum Cα-Cα distance spanned by the cross-linking reagent.

in close proximity to the conserved sensor loops adjacent to the subunit tails (Fig. 4D and table S12) (*16*). In a recent x-ray study on the tubulin-TRiC complex, these loops have been implicated in substrate interactions, and such contacts may trigger the adenosine triphosphate–driven conformational cycle (*35*). We performed cryo-electron microscopy (cryo-EM) analysis of the human 2ABG-TRiC complex isolated in an undefined nucleotide state by applying eight fold symmetry averaging. Three-dimensional (3D) reconstruction revealed a complex 145 Å in height and 160 Å in diameter at 23 Å resolution (Fig. 4D and fig. S14) (*16*). One ring was in an intermediate conformation between the closed and open states, whereas the other exhibited a fully open conformation, similar to the previously observed conformation of group II chaperonins in the presence of adenosine diphosphate or in nucleotide-free states (*32*). A globular density was found inside the central cavity at the equatorial domains, consistent with the localization for 2ABG inferred from cross-link distance restraints. Similarly, tubulin is bound to the equatorial domains in the tubulin-TRiC crystal structure (*35*). Additional density was also observed at the apical domains of the fully open ring, which might be attributed to a residual density of the disordered apical domains or to a protein not resolved by XL-MS. Our results provide further evidence for interactions of TRiC with substrate protein at the bottom of the cavity. In contrast, the bacterial group I chaperonin GroEL appears to exclusively recognize substrates with its apical domains (*36*, *37*).

The identification of cross-linked peptides by our mass spectrometry workflow yielded inter-residue distances that delineated the topology of a PP2A network in human cells. Molecular modeling and docking supported the integration of complementary structural data that facilitated the localization of the binding interface between IGBP1 and the catalytic subunits of PP2A and PP4 and suggested a mode for targeting the PP2A inhibitor SET to the catalytic center by the PP2A cell cycle adaptor protein SGOL1. Interprotein cross-links were sufficient to describe the subunit topology of the 1-MDa complex TRiC and uncovered the localization of the substrate 2ABG at the equatorial domains of TRiC subunits. This study demonstrates the applicability of XL-MS to acquire structural data from heterogeneous protein preparations in a systematic manner and highlights the potential of hybrid structural biology approaches (*38*) that integrate cross-link–derived

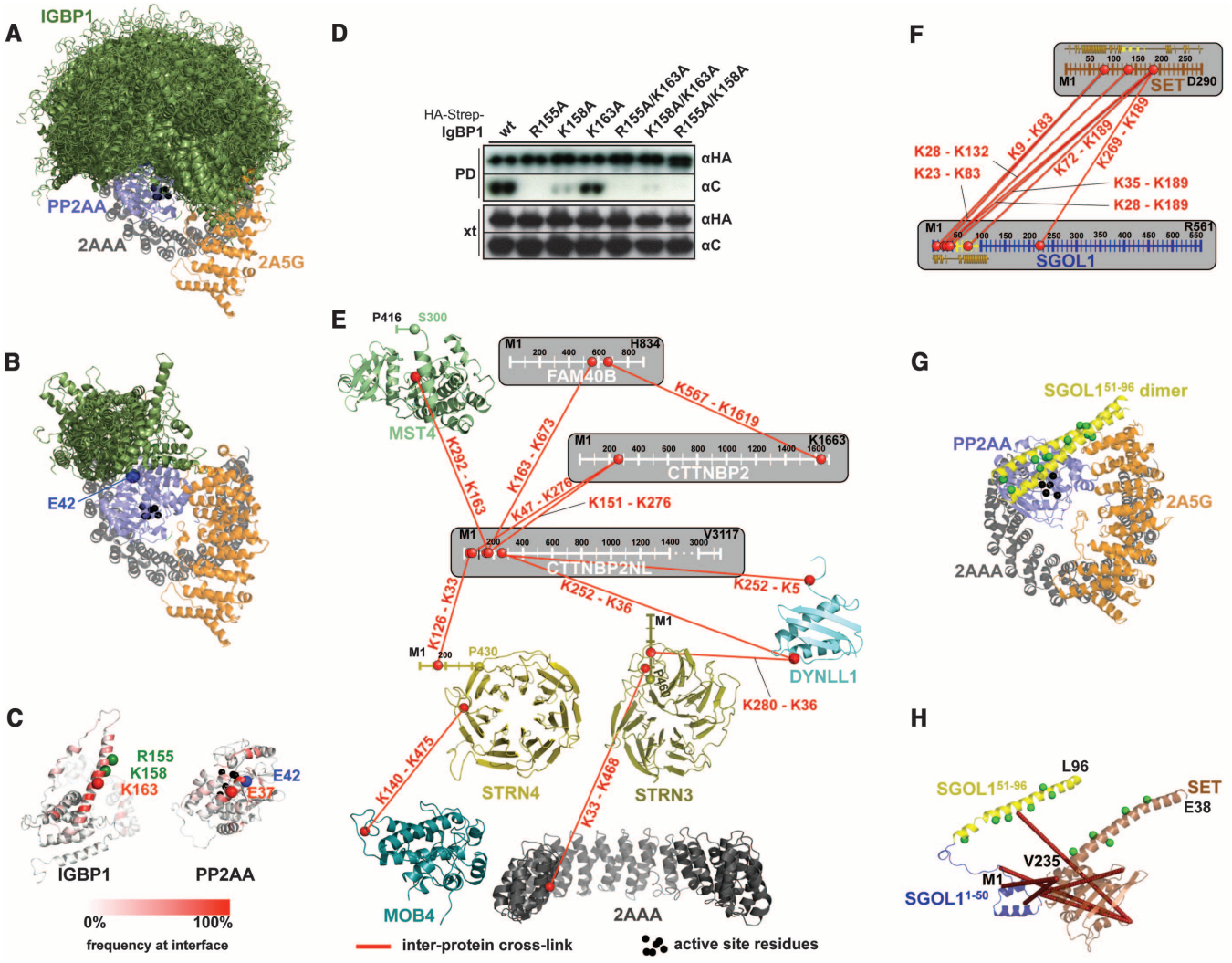

Fig. 3. Topology of PP2A-associated protein complexes by applying cross-links to guide computational modeling and docking. (**A** to **C**) Identification of the IGBP1-PP2AA binding interface using distance restraints in protein-protein docking experiments (*13*). (A) Docking models of IGBP1 and PP2AA by superimposing 237 IGBP1 cluster representatives (green) on a PP2AA/2AAA/2A5G complex (PDB entry 3FGA). (B) Four cluster representatives of IGBP1-PP2AA docking models with the shortest average distance for interprotein cross-links. (C) Frequency of amino acid residues mapped to the interface in IGBP1-PP2AA docking models. (**D**) Pull-down (PD) binding assay. IGBP1 wild-type and mutant proteins were affinity-purified from human cell extracts (xt), and binding of PP2A catalytic (C) subunits was analyzed by immunoblotting. (**E**) Schematic subunit map of the STRIPAK complex based on interprotein cross-links. (**F**) Interprotein cross-links detected on a complex of SGOL1 and SET suggest an antiparallel arrangement. (**G**) Hydrophobic residues (green spheres) essential for SGOL1 homodimerization (PDB entry 3FGA). (**H**) Scheme of SGOL1 in complex with SET based on cross-links. Green spheres, hydrophobic residues.

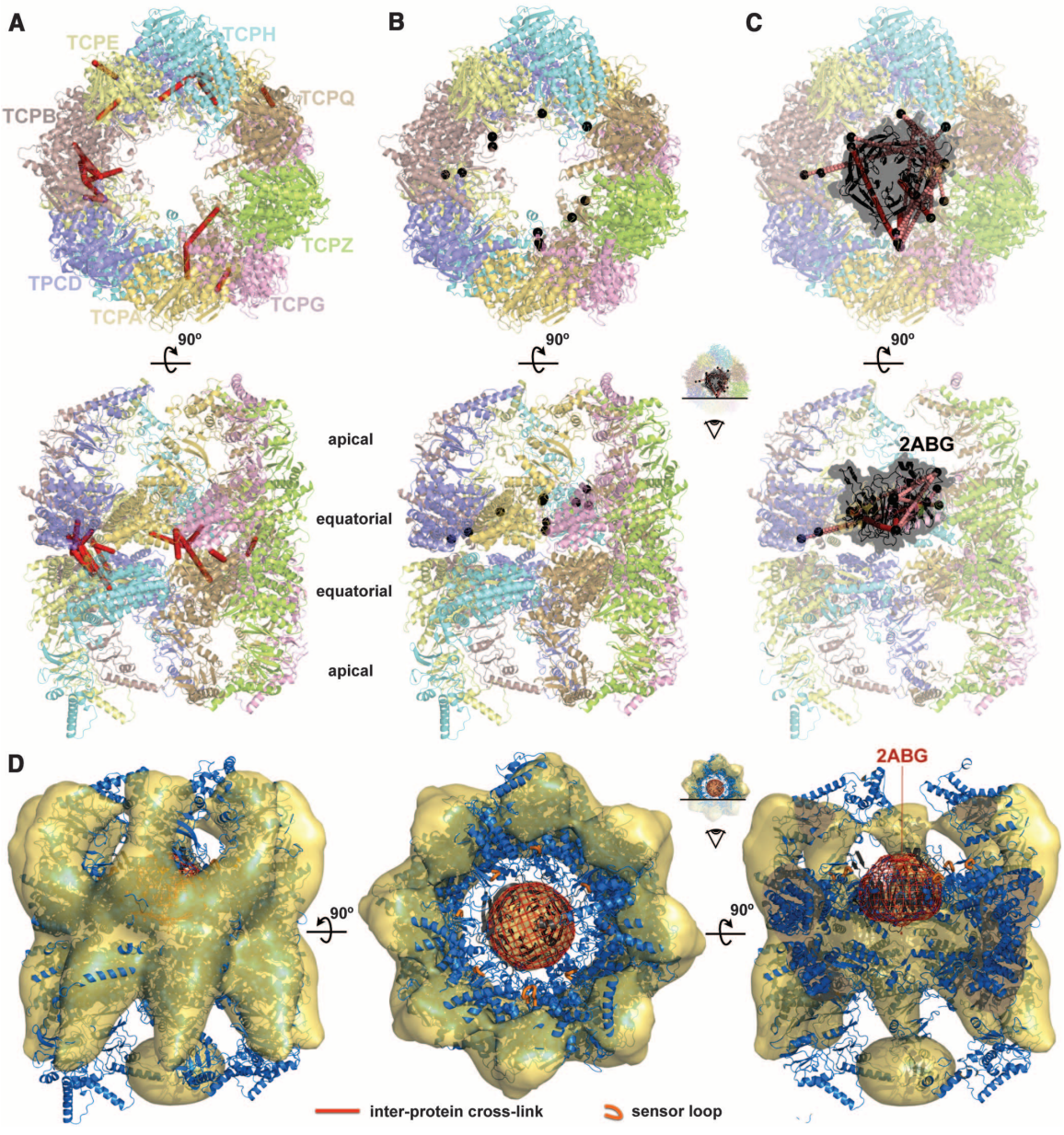

Fig. 4. Architecture of the TRiC chaperonin bound to its substrate 2ABG. (**A**) The subunit register of the two stacked TRiC rings was indicated by 19 inter-ring cross-links. (**B**) Eleven lysine residues (black spheres) within six TRiC subunits were cross-linked to 2ABG. (**C**) Schematic model of TRiC in complex with its substrate 2ABG based on cross-links. (**D**) Cryo-EM 3D-reconstruction of the 2ABG-TRiC complex. The comparative model of human TRiC (blue) was fitted into the EM 3D structure of TRiC (yellow). A globular density (red mesh representation) was located at the 2ABG position inferred from cross-links.

distance restraints and high-resolution structural information with computational molecular modeling.

References and Notes

1. F. Alber *et al.*, *Nature* **450**, 695 (2007).
2. P. Aloy, R. B. Russell, *Nat. Rev. Mol. Cell Biol.* **7**, 188 (2006).
3. A. Leitner *et al.*, *Mol. Cell. Proteomics* **9**, 1634 (2010).
4. H. Zhang *et al.*, *Mol. Cell. Proteomics* **8**, 409 (2009).
5. Z. A. Chen *et al.*, *EMBO J.* **29**, 717 (2010).
6. S. Jennebach, F. Herzog, R. Aebersold, P. Cramer, *Nucleic Acids Res.* **40**, 5591 (2012).
7. K. Lasker *et al.*, *Proc. Natl. Acad. Sci. U.S.A.* **109**, 1380 (2012).
8. M. A. Lauber, J. P. Reilly, *Anal. Chem.* **82**, 7736 (2010).
9. V. Janssens, J. Goris, *Biochem. J.* **353**, 417 (2001).
10. G. B. Moorhead, L. Trinkle-Mulcahy, A.Ulke-Lemée, *Nat. Rev. Mol. Cell Biol.* **8**, 234 (2007).
11. Y. Shi, *Cell* **139**, 468 (2009).
12. C. Wurzenberger, D. W. Gerlich, *Nat. Rev. Mol. Cell Biol.* **12**, 469 (2011).
13. D. M. Virshup, S. Shenolikar, *Mol. Cell* **33**, 537 (2009).
14. M. Goudreault *et al.*, *Mol. Cell. Proteomics* **8**, 157 (2009).
15. J. R. Hutchins *et al.*, *Science* **328**, 593 (2010).
16. Materials and methods are available as supplementary materials on *Science* Online.
17. A. Leitner *et al.*, *Mol. Cell. Proteomics* **11**, M111.014126 (2012).
18. O. Rinner *et al.*, *Nat. Methods* **5**, 315 (2008).
19. A. Wepf, T. Glatter, A. Schmidt, R. Aebersold, M. Gstaiger, *Nat. Methods* **6**, 203 (2009).
20. Y. Xu *et al.*, *Cell* **127**, 1239 (2006).
21. M. Kong, D. Ditsworth, T. Lindsten, C. B. Thompson, *Mol. Cell* **36**, 51 (2009).
22. T. D. Prickett, D. L. Brautigan, *J. Biol. Chem.* **279**, 38912 (2004).
23. M. LeNoue-Newton *et al.*, *J. Biol. Chem.* **286**, 17665 (2011).
24. H. Wang, X. Wang, Y. Jiang, *Mol. Biol. Cell* **14**, 4342 (2003).
25. P. Bradley, D. Baker, *Proteins* **65**, 922 (2006).
26. J. J. Gray *et al.*, *J. Mol. Biol.* **331**, 281 (2003).
27. X. Yan, R. Habedanck, E. A. Nigg, *Mol. Biol. Cell* **17**, 634 (2006).
28. T. S. Kitajima *et al.*, *Nature* **441**, 46 (2006).
29. C. G. Riedel *et al.*, *Nature* **441**, 53 (2006).
30. Z. Xu *et al.*, *Mol. Cell* **35**, 426 (2009).
31. S. Muto *et al.*, *Proc. Natl. Acad. Sci. U.S.A.* **104**, 4285 (2007).
32. Y. Cong *et al.*, *EMBO J.* **31**, 720 (2012).
33. N. Kalisman, C. M. Adams, M. Levitt, *Proc. Natl. Acad. Sci. U.S.A.* **109**, 2884 (2012).
34. A. Leitner *et al.*, *Structure* **20**, 814 (2012).
35. I. G. Muñoz *et al.*, *Nat. Struct. Mol. Biol.* **18**, 14 (2011).
36. L. Chen, P. B. Sigler, *Cell* **99**, 757 (1999).
37. D. K. Clare *et al.*, *Cell* **149**, 113 (2012).
38. F. Alber *et al.*, *Nature* **450**, 683 (2007).

Acknowledgments: We thank S. Hauri, A. Frei, and M. Gstaiger for support. Primary mass spectrometry data are available as mzXML files at www.peptideatlas.org/PASS/PASS00053. This work was supported by the EU FP7 project PROSPECTS. F.H. was supported by the European Molecular Biology Organization and by the European Commission (FP7-PEOPLE-IEF). R.A. was supported by the European Research Council advanced grant Proteomics v.3.0.

Supplementary Materials

www.sciencemag.org/cgi/content/full/337/6100/1348/DC1
Materials and Methods
Figs. S1 to S14
Tables S1 to S14
Boxes S1 to S9
References (*39*–*86*)

5 March 2012; accepted 18 July 2012
10.1126/science.1221483